RESEARCH ARTICLE SUMMARY

MOLECULAR BIOLOGY

The ZSWIM8 ubiquitin ligase mediates target-directed microRNA degradation

Charlie Y. Shi, Elena R. Kingston, Benjamin Kleaveland, Daniel H. Lin, Michael W. Stubna, David P. Bartel*

INTRODUCTION: MicroRNAs (miRNAs) are short RNAs that direct widespread gene repression in the cells of humans and other animals. Each miRNA associates with an Argonaute (AGO) protein to form a silencing complex in which the miRNA pairs to sites within target mRNAs, and AGO recruits machinery that causes destabilization or reduced translation of the targeted transcript. In the aggregate, miRNAs reduce the output of most human genes, and most of the 90 broadly conserved miRNA families found in mammals are required for viability or proper development.

Most miRNAs are quite long-lived because association with AGO protects them from cellular nucleases. However, some miRNAs are relatively unstable. A potential explanation for the instability of these miRNAs comes from the observation that interactions with certain target sites can promote miRNA destruction, thereby inverting the typical regulatory logic. This phenomenon of target-directed miRNA degradation (TDMD) is exploited by some viruses, which produce transcripts that trigger the decay of specific host miRNAs that would otherwise impede viral replication. In addition, four endogenous transcripts have recently been found to trigger TDMD. These include the CYRANO long noncoding RNA, which directs efficient degradation of miR-7. However, the extent to which this phenomenon might accelerate the degradation of other miRNAs has been unclear, in part because proteins required for TDMD had not been identified.

RATIONALE: The unusual target sites that trigger TDMD differ from the typical sites that mediate gene repression in that they not only pair to the 5′ region of the miRNA but also pair extensively to the miRNA 3′ region. This extensive pairing to the 3′ region can cause conformational changes that expose the miRNA 3′ terminus to enzymes that append or remove nucleotides—processes called tailing and trimming, respectively. The tailing and trimming observed in the presence of sites that trigger TDMD have been proposed to be obligate steps of the TDMD pathway. However, loss of an enzyme responsible for target-directed tailing has little influence on CYRANO-directed degradation of miR-7, which suggests that TDMD might occur through another mechanism. To learn more about this mechanism, we carried out a CRISPRi screen designed to identify proteins required for CYRANO-directed degradation of miR-7 in cultured human cells.

RESULTS: Our screen revealed that the ZSWIM8 protein was required for CYRANO-directed miR-7 degradation. ZSWIM8 was also required for other known examples of TDMD, including degradation triggered by a viral noncoding RNA and a cellular mRNA. Moreover, identification of miRNAs that increased after knocking out *ZSWIM8* in different types of mouse and human cells implicated dozens of additional miRNAs as substrates of endogenous TDMD. Indeed, for cells in which miRNA half-lives were known, TDMD explained the destabilization of most short-lived miRNAs. Similar experiments that examined the consequences of knocking out the *ZSWIM8* ortholog in *Drosophila* cells and nematodes indicated that endogenous TDMD also shapes miRNA levels and dynamics in invertebrate species.

ZSWIM8 is the substrate receptor of a Cullin-RING E3 ubiquitin ligase; this suggests an alternative model for TDMD that does not depend on miRNA tailing and trimming. In this model, the ZSWIM8 ubiquitin ligase recognizes the conformational changes that occur upon extensive pairing to the miRNA 3′ region, which leads to polyubiquitination of AGO. Polyubiquitinated AGO is then degraded by the 26*S* proteasome, thereby exposing the miRNA to cytoplasmic nucleases. In support of this model, knockdown of other known components of the ZSWIM8 ubiquitin ligase impeded TDMD, as did inhibition of ubiquitin activation, of general Cullin-RING ligase activity, or of proteasome-mediated proteolysis. Moreover, the miRNAs that were TDMD substrates preferentially associated with polyubiquitinated proteins in the presence of ZSWIM8, and substitutions of lysines on the surface of AGO abrogated TDMD, which implicates AGO as the direct target of the ubiquitin ligase.

CONCLUSION: The finding that TDMD requires the ZSWIM8 ubiquitin ligase supports a model of TDMD in which target-directed proteolysis of AGO exposes the miRNA for degradation. Furthermore, the implied scope of TDMD extends far beyond the four endogenous examples previously identified in mammals and other vertebrates. Endogenous TDMD appears to influence dozens of miRNAs in mammalian cells, and it extends to *Drosophila* and nematodes, which suggests that it has been shaping miRNA levels and dynamics since the last common ancestor of bilaterian animals. ■

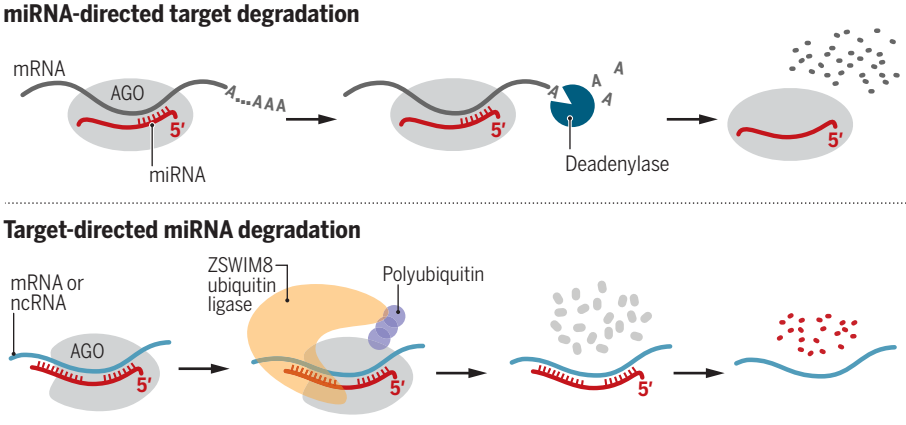

Molecular models for effects of miRNAs on targets, and vice versa. During miRNA-mediated regulation (top), the miRNA directs AGO to an mRNA, which recruits proteins that shorten the mRNA poly(A) tail, causing more rapid mRNA degradation. During TDMD (bottom), a target site with extensive pairing to the miRNA 3′ region induces conformational changes that are recognized by the ZSWIM8 ubiquitin ligase. This ligase polyubiquitinates AGO, causing its proteolysis, which exposes the miRNA for degradation. ncRNA, noncoding RNA.

The list of author affiliations is available in the full article online.
*Corresponding author. Email: dbartel@wi.mit.edu
Cite this article as C. Y. Shi *et al.*, *Science* **370**, eabc9359 (2020). DOI: 10.1126/science.abc9359

READ THE FULL ARTICLE AT
https://doi.org/10.1126/science.abc9359

RESEARCH ARTICLE

MOLECULAR BIOLOGY

The ZSWIM8 ubiquitin ligase mediates target-directed microRNA degradation

Charlie Y. Shi[1,2,3], Elena R. Kingston[1,2,3], Benjamin Kleaveland[4], Daniel H. Lin[1,2,3], Michael W. Stubna[1,2,3], David P. Bartel[1,2,3]*

MicroRNAs (miRNAs) associate with Argonaute (AGO) proteins to direct widespread posttranscriptional gene repression. Although association with AGO typically protects miRNAs from nucleases, extensive pairing to some unusual target RNAs can trigger miRNA degradation. We found that this target-directed miRNA degradation (TDMD) required the ZSWIM8 Cullin-RING E3 ubiquitin ligase. This and other findings support a mechanistic model of TDMD in which target-directed proteolysis of AGO by the ubiquitin-proteasome pathway exposes the miRNA for degradation. Moreover, loss-of-function studies indicated that the ZSWIM8 Cullin-RING ligase accelerates degradation of numerous miRNAs in cells of mammals, flies, and nematodes, thereby specifying the half-lives of most short-lived miRNAs. These results elucidate the mechanism of TDMD and expand its inferred role in shaping miRNA levels in bilaterian animals.

MicroRNAs (miRNAs) are ~22-nucleotide (nt) RNAs that pair to sites in mRNAs, thereby causing more rapid degradation and/or translational repression of these mRNA targets (*1*, *2*). In the aggregate, miRNAs regulate most human mRNAs (*3*), and most of the 90 broadly conserved miRNA families found in mammals are required for viability or proper development (*1*). Whereas mRNAs typically decay after only a few hours, most miRNAs persist much longer—often longer than a day and sometimes longer than a week (*4*–*6*). This stability is explained by the residence of each miRNA within an effector protein, Argonaute (AGO), which interacts with the miRNA throughout its length, thereby protecting it from nucleases (*7*, *8*).

Despite the stability of most miRNAs, some can be relatively short-lived, with half-lives ranging from <2 hours to 10 hours (*4*, *5*, *9*). A potential explanation for these shorter half-lives comes from the observation that pairing between a miRNA and an unusually highly complementary target can trigger decay of the miRNA, inverting the typical regulatory logic. This phenomenon, termed target-directed miRNA degradation (TDMD), was initially observed after introducing either antisense miRNA inhibitors or artificial targets with extensive pairing into cells (*10*–*14*), or after infection by some herpesviruses, which express transcripts with extensively paired sites that direct the degradation of host antiviral miRNAs (*15*–*18*). More recently, four cellular transcripts have also been found to trigger TDMD (*19*–*21*). For example, the Cyrano long noncoding RNA (lncRNA) directs efficient degradation of the miR-7 miRNA (*21*). After either deleting *Cyrano* or mutating the site within Cyrano that pairs extensively to miR-7 (Fig. 1A), steady-state miR-7 levels increase by as much as a factor of 50 in some cells and tissues (*4*, *21*). Moreover, after loss of Cyrano, the half-life of miR-7 increases to resemble that of most other miRNAs (*4*).

In contrast to the extensively paired sites that trigger TDMD (e.g., Fig. 1A), most miRNA regulatory sites pair only to the miRNA seed region (2 to 8 nt from the miRNA 5′ terminus) (*22*). Some sites also possess supplementary pairing, but this pairing is less common (conserved in only 5% of the preferentially conserved sites) and rarely approaches the miRNA 3′ terminus (*22*), which explains why most regulatory sites do not trigger TDMD.

Some sites that trigger TDMD also cause addition of untemplated nucleotides to the miRNA 3′ terminus and/or removal of 3′-terminal nucleotides, processes known as tailing and trimming, respectively (*8*, *12*–*14*, *17*, *19*–*21*, *23*–*26*). Mechanistically, the extensive 3′ pairing characteristic of these sites is proposed to promote conformational changes that separate the 3′ end of the miRNA from its binding pocket in the PAZ domain of AGO, thereby exposing it to cytosolic terminal nucleotidyltransferases and exonucleases (*12*). Consistent with this proposal, tailing and trimming each occur while the affected miRNA is still bound by AGO (*8*, *23*, *25*). Moreover, crystal structures reveal conformational changes in both the protein and the miRNA that accompany extensive pairing to the 3′ portion of the miRNA and indicate that these changes leave the miRNA 3′ terminus potentially vulnerable to enzymatic modification (*8*).

Taken together with the role of tailing in marking other RNA substrates for degradation (*27*–*35*), these findings have led to a model of TDMD whereby tailing marks the miRNA for trimming and, ultimately, degradation by cellular nucleases (*8*, *12*). However, any model that mechanistically couples target-directed tailing and trimming (TDTT) to TDMD is challenged by the observations that some miRNA sites trigger TDTT without detectable miRNA degradation (*8*, *12*), whereas others trigger TDMD without detectable tailing and trimming (*12*). Moreover, deletion of the gene encoding the PAPD4 (TENT2/TUT2/GLD2) terminal nucleotidyltransferase eliminates miR-7 tailing attributable to Cyrano yet has no detectable effect on Cyrano-directed miR-7 degradation (*21*).

A better understanding of the TDMD mechanism would benefit from the identification of proteins required for this phenomenon. Although TDMD was first described more than a decade ago, no such proteins have been reported. Because many candidates, including known terminal nucleotidyltransferases and nucleases, had already been tested for roles in either TDMD or miRNA turnover more generally (*9*, *21*, *25*, *26*, *36*–*38*), we set out to use an unbiased approach to identify proteins that function in the TDMD pathway.

ZSWIM8 is required for CYRANO-directed miR-7 degradation

To find factors required for TDMD, we developed a CRISPR screen designed to identify protein-coding genes needed to reduce the level of miR-7. The screen used CRISPR interference (CRISPRi), a gene-knockdown method in which KRAB-dCas9 [catalytically defective Cas9 (dCas9) fused at its N terminus to the Krüppel-associated box (KRAB) transcriptional repression domain] is ectopically expressed in cells and directed to the vicinity of transcription start sites by coexpressed guide RNAs (gRNAs) (*39*). After engineering K562 cells (a human erythroleukemia cell line) to express KRAB-dCas9, we further modified these cells to express two reporter mRNAs from a bidirectional promoter (Fig. 1B). One reporter was designed to report on cellular miR-7 activity; it contained two sites predicted to undergo miR-7–directed slicing and encoded the mCherry fluorescent protein. The other reporter was designed to normalize for expression independent of miR-7; it contained no miR-7 sites and encoded green fluorescent protein (GFP).

To confirm the utility of these cells, we transduced them with either a lentivirus expressing a control gRNA or one that expressed a gRNA that recruits KRAB-dCas9 to the *CYRANO* promoter and silences its transcription (*21*). As expected if cellular fluorescence reported on the efficacy of CYRANO-directed miR-7 degradation,

[1]Howard Hughes Medical Institute, Whitehead Institute for Biomedical Research, Cambridge, MA 02142, USA. [2]Whitehead Institute for Biomedical Research, Cambridge, MA 02142, USA. [3]Department of Biology, Massachusetts Institute of Technology, Cambridge, MA 02139, USA. [4]Department of Pathology and Lab Medicine, Weill Cornell Medicine, New York, NY 10065, USA.
*Corresponding author. Email: dbartel@wi.mit.edu

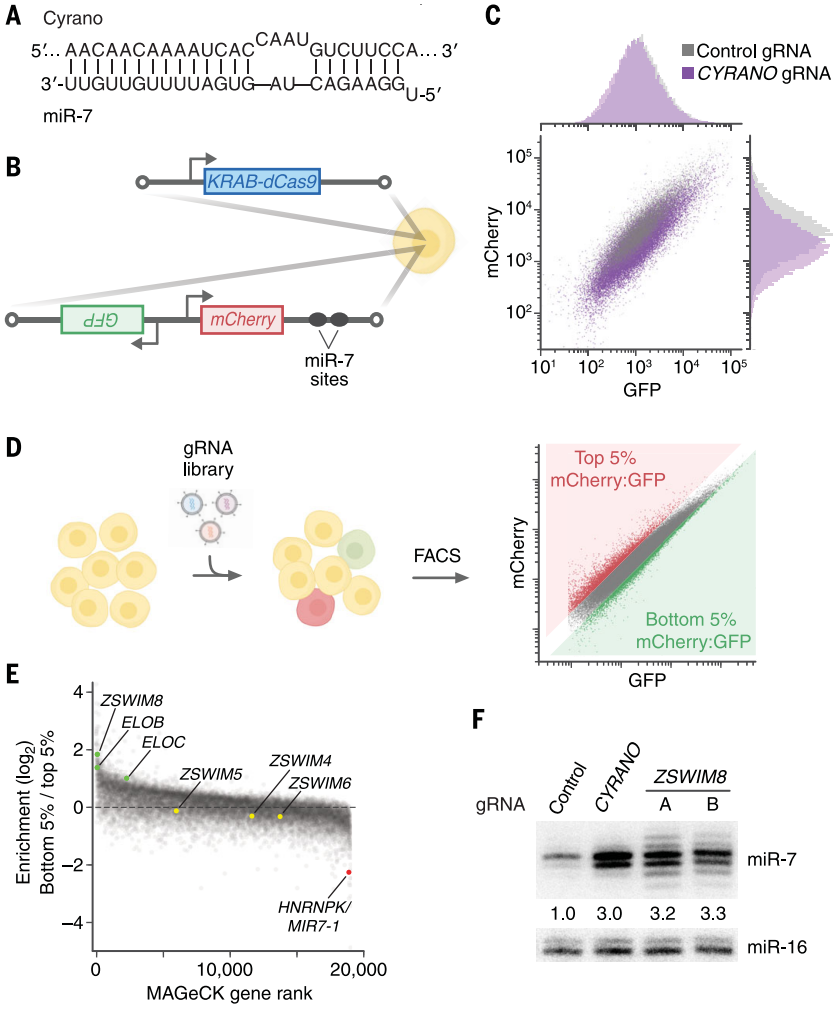

Fig. 1. A CRISPRi screen identifies ZSWIM8 as a regulator of miR-7. (**A**) The extensive complementarity between Cyrano and miR-7. Vertical lines indicate Watson-Crick complementarity, excluding the first nucleotide of the miRNA, which is not available for pairing (*1*). (**B**) The engineered K562 cell line used to perform the CRISPRi screen. This line was generated by stably integrating two constructs into the genome; one expressed *KRAB-dCas9*, and the other expressed *GFP* and *mCherry* reporter mRNAs from a bidirectional promoter. The *mCherry* mRNA had two sites in its 3′ untranslated region that were designed to be susceptible to miR-7–directed slicing. (**C**) Flow cytometry of cells in (B) transduced with lentiviral constructs expressing either a nontargeting control gRNA or a gRNA targeting *CYRANO* for knockdown. (**D**) Schematic of the genome-wide CRISPRi screen. Cells in (B) were transduced with a lentiviral CRISPRi gRNA library, cultured, and sorted with respect to their mCherry:GFP ratios, collecting cells with ratios in the top 5% and bottom 5% of all cells. The abundances of gRNAs in these two populations were then determined by high-throughput sequencing. FACS, fluorescence-activated cell sorting. (**E**) Results of the screen. Aggregate gRNA enrichment in cells with mCherry:GFP ratios in the bottom 5%, relative to that in cells with ratios in the top 5%, is plotted as function of MAGeCK rank. (**F**) Influence of ZSWIM8 on miR-7 accumulation. Shown is a representative RNA blot measuring miR-7 and miR-16 levels in an independently derived K562i line expressing either a nontargeting control gRNA, a gRNA targeting *CYRANO*, or one of two gRNAs (A and B) targeting *ZSWIM8* for CRISPRi-mediated knockdown. miR-7 levels were normalized to those of miR-16, and mean levels relative to that observed for the nontargeting control are shown; n = 3 biological replicates.

transduction with the *CYRANO* gRNA caused mCherry:GFP ratios to drop (Fig. 1C), which presumably reflected reduced CYRANO-directed miR-7 degradation, leading to increased miR-7 accumulation and thus reduced mCherry expression. Having confirmed the desired response, albeit with relatively low magnitude, we went forward with the screen. The reporter cells were transduced with the CRISPRi v2 lentiviral library designed to express 10 gRNAs per protein-coding gene (Fig. 1D) (*40*). After 10 days of culture, cells were sorted, collecting populations at the bottom 5% and the top 5% with respect to the mCherry:GFP ratio (Fig. 1D), which were expected to be enriched and depleted, respectively, in cells with increased miR-7 accumulation. The gRNA cassettes from these two populations were sequenced, and genes that were preferentially targeted in the bottom 5% relative to the top 5% were identified by the MAGeCK algorithm, which statistically scores gRNA enrichment for each gene (*41*) (Fig. 1E, fig. S1B, and data S1).

Among the 70 genes with a false discovery rate (FDR) of ≤0.3 (data S1), 56 candidates were selected for a secondary screen that more directly queried the influence on miR-7 levels. For each candidate, gRNAs were expressed in K562i cells (an independent K562 cell line competent for CRISPRi) (*42*), and an RNA blot was used to detect an increase in miR-7 without a change in either the pre-miRNA hairpin or a control miRNA (fig. S1A). This secondary screen validated a single candidate: Knockdown of *ZSWIM8* with either gRNA caused an increase in miR-7, with magnitude resembling that of the *CYRANO* knockdown (Fig. 1F and fig. S1A). Likewise, Cas9-mediated knockout of *ZSWIM8* caused increased miR-7, and as expected, expression of wild-type ZSWIM8 in the knockout background restored the normal miR-7 level (fig. S1C; DNA lesions of this and other clonal knockout lines are listed in table S1A).

ZSWIM8 acts in miR-7 degradation downstream of CYRANO

High-throughput sequencing of small RNAs isolated from K562i cells further established the similarities between the functions of ZSWIM8 and CYRANO, showing that miR-7 levels specifically increased upon either *ZSWIM8* knockdown or *ZSWIM8* knockout, as also observed upon *CYRANO* knockdown (Fig. 2A, fig. S2A, table S1A, and data S2). These small-RNA sequencing (sRNA-seq) results also provided the opportunity to monitor the effect of ZSWIM8 on the level of the miR-7 passenger strand. MicroRNA biogenesis culminates in the production of a miRNA duplex, consisting of a miRNA and its passenger strand. This duplex associates with AGO in a manner that retains one strand—typically the one annotated as the miRNA—as the guide strand and expels the passenger strand, which is rapidly degraded. sRNA-seq showed that despite the increase in miR-7 observed upon *ZSWIM8* knockdown, the level of its passenger strand did not significantly change (Fig. 2A). This increase in miRNA, with no change in its passenger strand, was also observed after loss of CYRANO (Fig. 2A) (*21*) and would be expected after knockdown of a TDMD factor because TDMD acts after the miRNA is loaded into AGO and thus affects only the guide strand. In contrast, most other processes that influence miRNA levels (such as differential transcription or processing) affect accumulation of both guide and passenger strands. Thus, this behavior of miR-7 and its passenger strand supported the idea that our CRISPRi screen had identified a protein

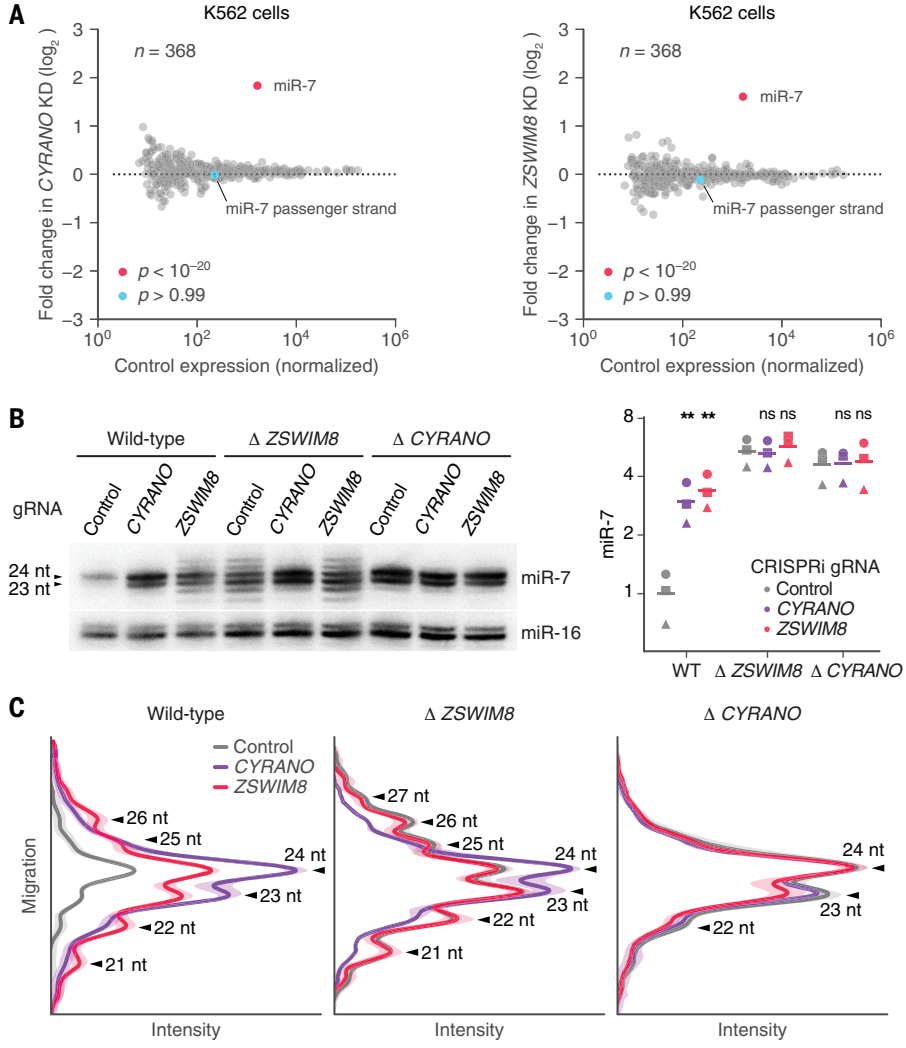

Fig. 2. *ZSWIM8* is required for target-directed miR-7 degradation, acting downstream of *CYRANO*. (**A**) Influence of CYRANO and ZSWIM8 on miRNA levels in K562i cells. Shown are relative (fold) changes in mean miRNA levels observed upon CRISPRi-mediated knockdown of either *CYRANO* (left) or *ZSWIM8* (right). Relative miRNA levels measured by sRNA-seq after knockdown were compared with those observed after expressing a control gRNA (n = 3 biological replicates). The point for the miRNA that significantly changed (adjusted p value < 10^{-7}, as determined by DESeq2) is indicated (red), as is the point for its passenger strand (blue). (**B**) Genetic interaction between *CYRANO* and *ZSWIM8*. Left: RNA blot measuring miR-7 and miR-16 levels in clonal K562i lines in which the indicated gene had been knocked out (wild type, Δ*CYRANO*, and Δ*ZSWIM8*; table S1A) and either a nontargeting control gRNA, a gRNA targeting *CYRANO*, or a gRNA targeting *ZSWIM8* (gRNA B) was expressed for CRISPRi-mediated knockdown (fig. S2C). Right: Results of quantification of this blot (squares), measuring miR-7 normalized to miR-16, plotted together with results from two additional biological replicates, each performed with independent control or knockout clonal lines (circles and triangles; means, horizontal lines). All values were normalized to the loading control (miR-16), then to hybridization standards, and finally to the mean of WT expressing the control gRNA. **p < 0.005 (two-tailed paired ratio t test of fold changes between cells expressing targeting and control gRNAs within the same genetic background); ns, not significant. (**C**) Influence of CYRANO and ZSWIM8 on miR-7 length variation. Plotted are intensity values (arbitrary units) as a function of gel migration (arbitrary units) measured by line densitometry of RNA blots in (B) and its biological replicate. Peaks correspond to lengths of miR-7 isoforms, as indicated (arrowheads). Shaded areas denote 95% confidence intervals across biological replicates (n = 2).

required for CYRANO-directed miR-7 degradation in K562 cells.

One way that ZSWIM8 might influence CYRANO-directed miR-7 degradation is by affecting *CYRANO* expression. For example, if ZSWIM8 were required for transcription of CYRANO, then knockdown of *ZSWIM8* would phenocopy knockdown of *CYRANO*. However, RNA sequencing (RNA-seq) analyses showed that *ZSWIM8* knockdown had no detectable effect on CYRANO levels, and vice versa, thereby excluding the possibility that ZSWIM8 affects CYRANO expression (fig. S2B). To investigate the hypothesis that ZSWIM8 and CYRANO nonetheless act in the same genetic pathway, we knocked down *ZSWIM8* in *CYRANO*-knockout cells and reciprocally knocked down *CYRANO* in *ZSWIM8*-knockout cells (fig. S2C). Whereas individual loss of either ZSWIM8 or CYRANO function caused miR-7 levels to increase, neither combination of perturbations caused any additional increase (Fig. 2B). Thus, ZSWIM8 and CYRANO each require the presence of the other to influence miR-7 levels and are part of the same pathway.

Although ZSWIM8 and CYRANO each had a similar effect on the total level of miR-7, *ZSWIM8* knockdown did not precisely phenocopy *CYRANO* knockdown. The distribution of miR-7 isoforms observed upon *ZSWIM8* knockdown was much broader than that observed upon *CYRANO* knockdown (Fig. 1F and Fig. 2, B and C). Analysis of sRNA-seq results confirmed that this length variability was specific to the miR-7 guide strand and occurred at its 3′ end—a hallmark of tailing and trimming (fig. S3). These distinct molecular phenotypes provided the opportunity to perform epistasis analyses to order CYRANO and ZSWIM8 in the pathway. The reduced extent of tailing and trimming observed upon combining a *CYRANO* knockout with a *ZSWIM8* knockdown (or a *CYRANO* knockdown with a *ZSWIM8* knockout) resembled that observed for the knockout (or knockdown) of only *CYRANO* (Fig. 2, B and C). Thus, CYRANO lies upstream of ZSWIM8 in the pathway, and CYRANO but not ZSWIM8 is required for miR-7 tailing and trimming.

We also explored the effects of other genes on the extensive tailing and trimming observed upon *ZSWIM8* knockout. Knockdown of *PARN* and *DIS3L2* in *ZSWIM8*-knockout cells did not reveal a substantial role for these nucleases in miR-7 trimming (fig. S2D). However, knockdown of *PAPD4* in *ZSWIM8*-knockout cells caused tailed species to decrease and trimmed species to increase, with no change in overall levels of miR-7. This finding confirmed the role of the PAPD4 terminal nucleotidyltransferase in miR-7 tailing (*21*) and indicated that trimmed species were not degradation intermediates downstream of tailing (fig. S2D). Moreover, building on the observation that a miRNA loaded into any of the four AGO paralogs (AGO1 to AGO4) can undergo TDTT (*8*), we found that miR-7 loaded into any of the four AGO paralogs could undergo ZSWIM8-dependent TDMD (fig. S2E).

ZSWIM8 and TDMD have widespread influence

Having found that ZSWIM8 is required for CYRANO-directed miR-7 degradation, we examined whether it might also be required for other instances of TDMD. *ZSWIM8* mRNA is

broadly expressed in human tissues, with a median of 45.2 TPM (transcripts per million) in a human transcript-expression atlas (fig. S4A) (*43*), which implies that it could be acting in many cell types to cause target-directed degradation of other miRNAs.

The founding biological example of TDMD is directed by *Herpesvirus saimiri* HSUR1, a 143-nt viral noncoding RNA that triggers the decay of host miR-27a (*8*, *15*). To examine the potential requirement of ZSWIM8 for HSUR1-directed miR-27a degradation, we knocked out *ZSWIM8* in BJAB cells (a human Burkitt lymphoma B cell line) engineered to express HSUR1 (*8*, *15*). Polyclonal knockout of *ZSWIM8* restored miR-27a levels in HSUR1-expressing cells but had no detectable effect on miR-27a levels in control lines that expressed either no additional RNA (empty vector) or a mutant HSUR1 unable to direct miR-27a degradation (Fig. 3A; efficiencies of these and other polyclonal knockouts are listed in table S1B). Probing for other miRNAs showed that, as expected, ZSWIM8 influenced miR-7 levels regardless of whether HSUR1 was present and had no influence on miR-20, which was not a suspected TDMD substrate in BJAB cells (Fig. 3A). Similar experiments indicated that *NREP*-directed degradation of miR-29b, the founding example of TDMD triggered by an endogenous mRNA (*19*), also depended on ZSWIM8 (fig. S4B).

The finding that ZSWIM8 was required for known instances of TDMD raised the prospect that additional miRNAs might be implicated as TDMD substrates on the basis of their increased accumulation after ZSWIM8 loss. Reasoning that the most affected miRNAs would be those with the shortest half-lives, we first tested miR-503, which has a relatively short half-life in mouse fibroblasts (*4*, *9*). miR-503 levels increased after polyclonal knockout of *Zswim8* (the mouse ortholog of the human *ZSWIM8* gene) in contact-inhibited NIH 3T3 cells, as would be expected if it is a TDMD

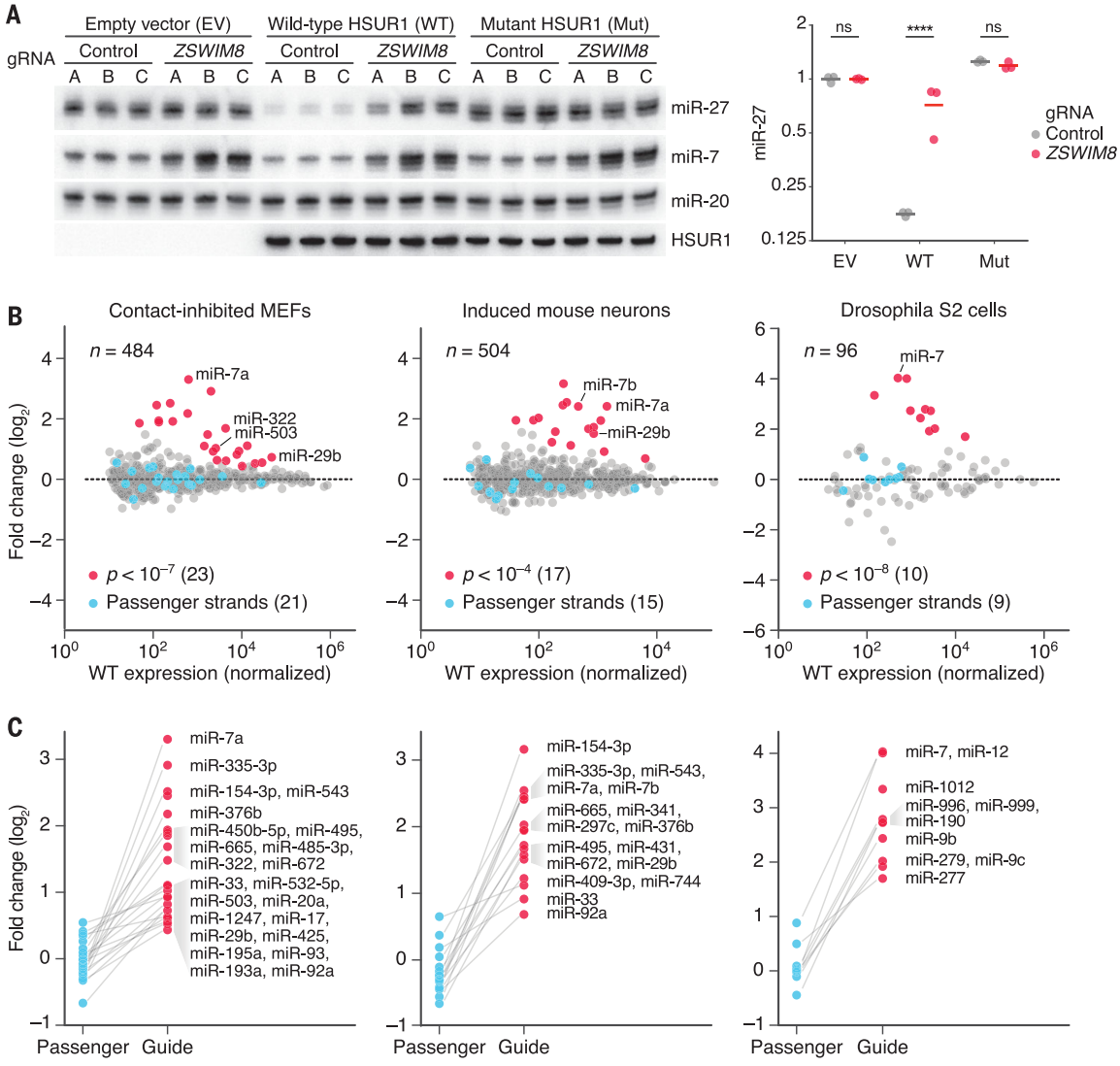

Fig. 3. ZSWIM8 is generally required for target-directed miRNA degradation (TDMD) and limits accumulation of many miRNAs in diverse species. (**A**) Requirement of ZSWIM8 for HSUR1-directed miR-27a degradation. The RNA blot measures levels of the indicated RNAs in BJAB cells stably expressing either HSUR1, mutant HSUR1, or empty vector—each also expressing Cas9 and either one of three control gRNAs (A, B, or C) or one of three gRNAs targeting *ZSWIM8* (A, B, or C) for polyclonal knockout (table S1B). The plot shows relative levels of miR-27 after normalizing to that of miR-20 and then to the mean level of cells expressing empty vector (EV) and control gRNAs (means, horizontal lines). ****$p <$ 0.0001 [two-way analysis of variance (ANOVA) followed by Bonferroni's multiple-comparisons test]. (**B**) The influence of ZSWIM8 on miRNA levels in cells from diverse species, as measured by sRNA-seq. Plotted are fold changes in miRNA levels observed upon polyclonal knockout of *Zswim8* in MEFs and induced mouse neurons, and clonal knockout of the *ZSWIM8* ortholog in *Drosophila* S2 cells (table S1). miRNA fold changes with significance exceeding the indicated *p*-value threshold are red; fold changes for their corresponding passenger strands are blue. miR-29b in MEFs and miR-7a in induced neurons each had two quantifiable passenger strands, whereas some other miRNAs did not have a passenger strand that exceeded our threshold for accurate quantification (data S2). Adjusted *p* values were determined by DESeq2. *n* = 3, 2, and 3 biological replicates for MEFs, induced mouse neurons, and S2 cells, respectively. Each replicate was performed with independent knockout and control lines (table S1A). (**C**) Asymmetric influence of ZSWIM8 on miRNA guide and passenger strands. Shown are the miRNA fold changes highlighted in (B), each paired with the fold change of its passenger strand(s). Unpaired points correspond to miRNAs for which passenger strands did not exceed the threshold for reliable quantification.

substrate (fig. S4C). We then looked more broadly for evidence of additional miRNAs subject to TDMD, using sRNA-seq to quantify changes in miRNA accumulation after polyclonal knockout of *Zswim8* in mouse embryonic fibroblasts (MEFs). To identify ZSWIM8-sensitive miRNAs, we considered different significance thresholds for differential expression, choosing $p < 10^{-7}$ as a value sufficiently permissive to capture increases in abundance upon *Zswim8* knockout, yet sufficiently stringent to avoid capturing any decreases. This approach identified 23 ZSWIM8-sensitive miRNAs. For these 23 miRNAs, 21 passenger strands could be reliably quantified, and in each case, the guide strand increased without a corresponding increase in its passenger strand(s)—as would be expected if each of these guides is a TDMD substrate (Fig. 3, B and C, and data S2). These 23 ZSWIM8-sensitive miRNAs included miR-7a (the murine miR-7 paralog expressed in MEFs) and miR-29b, as well as another 21 miRNAs not known to be TDMD substrates [including miR-503 and miR-322, which is related to miR-503 and is reported to have similar expression dynamics (*9*)]. Moreover, for most (20/21) of these additional ZSWIM8-sensitive miRNAs, the fraction of tailed and trimmed isoforms increased upon *Zswim8* knockout (fig. S4, D and E). Such increases would be expected if these miRNAs, like miR-7 and other known TDMD substrates (Fig. 2B and fig. S3A) (*8*), also pair to triggers in a manner that exposes their 3′ termini to tailing and trimming activities.

The identification of 23 ZSWIM8-sensitive miRNAs in MEFs contrasted with the single ZSWIM8-sensitive miRNA observed in K562 cells; this finding suggested that the scope of TDMD is much broader in some cells than in others. To examine a third mammalian cell type, we investigated the effects of polyclonal *Zswim8* knockout in neurons induced from mouse embryonic stem cells (mESCs). This analysis revealed 17 ZSWIM8-sensitive miRNAs, including miR-7a, miR-7b, miR-29b, and another nine miRNAs found to be ZSWIM8-sensitive in MEFs, as well as five additional newly identified ZSWIM8-sensitive miRNAs (Fig. 3, B and C, fig. S5A, and data S2). Similar analyses identified 10 ZSWIM8-sensitive miRNAs in human cancer lines, of which six were identified in the HeLa line, six in the MCF7 line, and four in the A549 line (originating from epithelia of cervix, breast, and lung, respectively) (fig. S5B and data S2). These 10 included miR-7, miR-29b, and orthologs of five other ZSWIM8-sensitive miRNAs found in mouse cells (fig. S5A). In sum, 32 ZSWIM8-sensitive miRNAs were identified in these mammalian cells (fig. S5A), which, when added to three TDMD substrates identified in other mammalian contexts (miR-30b, miR-30c, and miR-671) (*20*, *21*), brought the number of inferred TDMD substrates to 35.

The observation that some miRNAs were identified as TDMD substrates in some cells but not in others presumably reflected not only differential production of miRNAs in different cells, but also differential expression of their TDMD triggers. In support of this scenario, we found that differential expression of *NREP* (the mRNA that triggers miR-29b degradation) explained why miR-29b was identified as ZSWIM8-sensitive in some cells but not in others (fig. S5C).

We then extended our analyses beyond mammals, identifying 10 miRNAs sensitive to knockout of the *ZSWIM8* ortholog (*CG34401*) in *Drosophila* S2 cells, each of which increased without a corresponding increase in the passenger strand (Fig. 3, B and C, and data S2). These 10 included the *Drosophila* miR-7 ortholog, which suggested that targeted degradation of miR-7 might have been conserved since the bilaterian ancestor of flies and mammals. For each of these inferred TDMD substrates, the fraction of tailed and trimmed isoforms increased upon *CG34401* knockout (fig. S4E); these findings suggested that, as in mammals, endogenous TDMD in flies is triggered by targets that pair in a manner that exposes the miRNA 3′ termini to cytoplasmic tailing and trimming activities.

In *Caenorhabditis elegans* adult animals (which contain embryos), a null mutation in *ebax-1*, the *ZSWIM8* ortholog in nematodes (*44*), caused an increase in levels of 10 miRNAs, with no corresponding change in levels of their passenger strands (fig. S5D and data S2). These *ebax-1*–sensitive miRNAs included members of the miR-35 family. Given that expression of this family rapidly diminishes after embryos progress beyond the four-cell stage (*45*), our results imply that TDMD destabilizes members of the miR-35 family to help clear these miRNAs in older embryos. Other *ebax-1*–sensitive miRNAs are reported to increase during heat shock of stage 4 larva (fig. S5D) (*46*), which suggests that heat shock might inhibit the target-directed degradation normally occurring for these miRNAs.

In MEFs and S2 cells, two cell types in which miRNA half-lives have been globally measured (*4*, *5*), we found that the ZSWIM8-sensitive miRNAs tended to have shorter half-lives (Fig. 4A). Indeed, for these ZSWIM8-sensitive miRNAs, half-life values inversely correlated with ZSWIM8 sensitivity (r^2 = 0.79 in MEFs; r^2 = 0.45 in S2 cells), which supported the idea that ZSWIM8-mediated TDMD largely determines the half-lives of these short-lived miRNAs. To explore a causal relationship between ZSWIM8 and half-life, we examined the influence of ZSWIM8 on the decay of miR-503 and miR-322. When NIH 3T3 cells reenter the cell cycle after cell cycle arrest, the production of these miRNAs drops, and because they have relatively short half-lives, their levels decline rapidly (*9*). In *ZSWIM8* polyclonal knockout cells, levels of both miRNAs declined much less rapidly upon cell cycle reentry, which indicated that ZSWIM8 largely determines the half-lives of these two short-lived miRNAs (Fig. 4B).

Together, our global analyses of the effects of *ZSWIM8* disruption extend the inferred scope of endogenous TDMD far beyond the four miRNA families known as TDMD substrates in mammals and fish (*19*–*21*) to include dozens of miRNA families in mammals, flies, and worms. Indeed, in cells with measured miRNA half-lives, endogenous TDMD explains the rapid decay of most short-lived miRNAs.

The E3 model of TDMD

Although ZSWIM8 mediates TDMD, it does not appear to be a nuclease. Instead, ZSWIM8 is the substrate receptor of a Cullin-RING E3 ubiquitin ligase (CRL) (*44*). CRLs make up the largest class of E3 ubiquitin ligases, which often function to target specific proteins for ubiquitin-dependent degradation by the 26*S* proteasome (*47*). Each CRL contains a Cullin protein, which acts as a scaffold to link the substrate receptor with a RING-finger protein that binds E2 ubiquitin-conjugating enzymes, thereby promoting ubiquitination of the substrate (*48*). The ZSWIM8 CRL falls into an abundant subclass of CRLs that use Elongin B (ELOB/TCEB2) and Elongin C (ELOC/TCEB1) as adaptor proteins to help link the substrate receptor to a Cullin protein (*44*, *49*). Accordingly, ZSWIM8 has a Cullin box and a BC box, required for binding Cullin and the two Elongin proteins, respectively (Fig. 5A) (*44*). In addition, ZSWIM8 has a zinc-finger SWIM domain (a 35–amino acid domain initially recognized in the SWI/SNF2 chromatin remodeler and MuDR transposase), for which the protein is named, although no molecular function has been reported for this domain in ZSWIM8 (*50*). The Cullin box, BC box, and SWIM domain all fall within the first 208 amino acids of ZSWIM8, which spans 1837 amino acids in human (Fig. 5A). Although the remainder of the protein has no recognizable folds or motifs, ZSWIM8 is conserved broadly in animals throughout most of its length, with multiple expansive regions of high predicted order (Fig. 5A). This conserved and putatively structured remainder of the protein might help to recognize substrates and orient them for ubiquitination.

The biological functions of ZSWIM8 have been examined most extensively in *C. elegans*, where the ZSWIM8 ortholog is named EBAX-1 (Elongin BC-binding axon regulator). EBAX-1 is required for proper axon guidance, a function attributed to EBAX-1–directed degradation of misfolded SAX-3/Robo receptors in developing neurons (*44*). Our finding that EBAX-1 is also required for TDMD (fig. S5D) suggests that miRNA misregulation might also contribute to this phenotype. In flies, the

ZSWIM8 ortholog is required for viability, as indicated by the isolation of two lethal point substitutions (a missense allele and a nonsense allele) in a large-scale screen, which have not been further characterized (*51*). In human cells, ZSWIM8-dependent degradation of Robo, analogous to the EBAX-1–dependent degradation of *C. elegans* SAX-3, has been reported (*44*), but other functional analyses have been limited to genome-wide screens in cell lines. For example, results of CRISPR screens conducted in many cancer lines show that *ZSWIM8* is not required for cell viability but typically does impart a fitness advantage (*52*).

The discovery that ZSWIM8 is required for TDMD, together with the established function of ZSWIM8 as a CRL substrate receptor, suggested a revised model for the molecular mechanism of TDMD (Fig. 5B). In this model, ZSWIM8 specifically recognizes the conformational changes that occur as the TDMD trigger extensively pairs

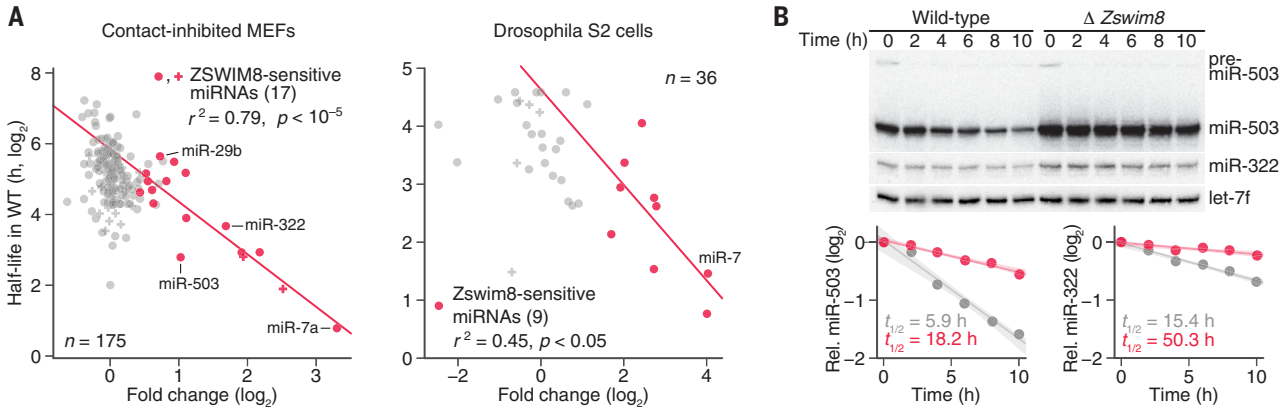

Fig. 4. TDMD explains the instability of most short-lived miRNAs. (**A**) Relationship between miRNA half-life and ZSWIM8 sensitivity. For each miRNA guide strand reliably quantified in contact-inhibited MEFs (left) or *Drosophila* S2 cells (right), its half-life in wild-type cells (*4*, *5*) is plotted as function of the fold change in its mean level observed upon loss of ZSWIM8, as quantified in Fig. 3B. If both strands of a miRNA duplex accumulated to similar levels (within a factor of 5 of each other in *Zswim8* knockout cells), implying that both strands commonly served as guide strands, then both strands were included in the analysis, with points indicated (+ instead of •). Points for ZSWIM8-sensitive miRNAs are colored red, as in Fig. 3B, and the line is the least-squares fit to these points (r^2, coefficient of determination; p value indicated). (**B**) Influence of ZSWIM8 on miRNA decay. Top: RNA blot measuring miR-503, miR-322, and let-7f levels in NIH 3T3 polyclonal lines expressing Cas9 and either a nontargeting control gRNA (wild-type) or a *Zswim8*-targeting gRNA (table S1B). Serum was reintroduced to serum-starved cultures, and samples were taken at the indicated times. Bottom: miR-503 and miR-322 levels in wild-type and Δ*Zswim8* cells (gray and red, respectively), after normalization to the loading control (let-7f) and the 0 time point of each cell line. Lines show the least-squares fit to the data (shading, 95% confidence interval), with apparent half-lives ($t_{1/2}$ values) derived from the fit also indicated; n = 1 biological replicate.

Fig. 5. The E3 model of TDMD and its interplay with TDTT. (**A**) The domain structure and conservation of human ZSWIM8. Annotated are the SWIM domain and known interaction motifs (*44*, *49*, *50*), predicted structural order and disorder (*58*), and relative amino acid conservation (arbitrary units) (*59*). (**B**) Schematic of the E3 model of TDMD and its interplay with TDTT (B, ELOB; C, ELOC; E2, ubiquitin-conjugating enzyme; RING, RING-finger protein; Ub, ubiquitin). See main text for description.

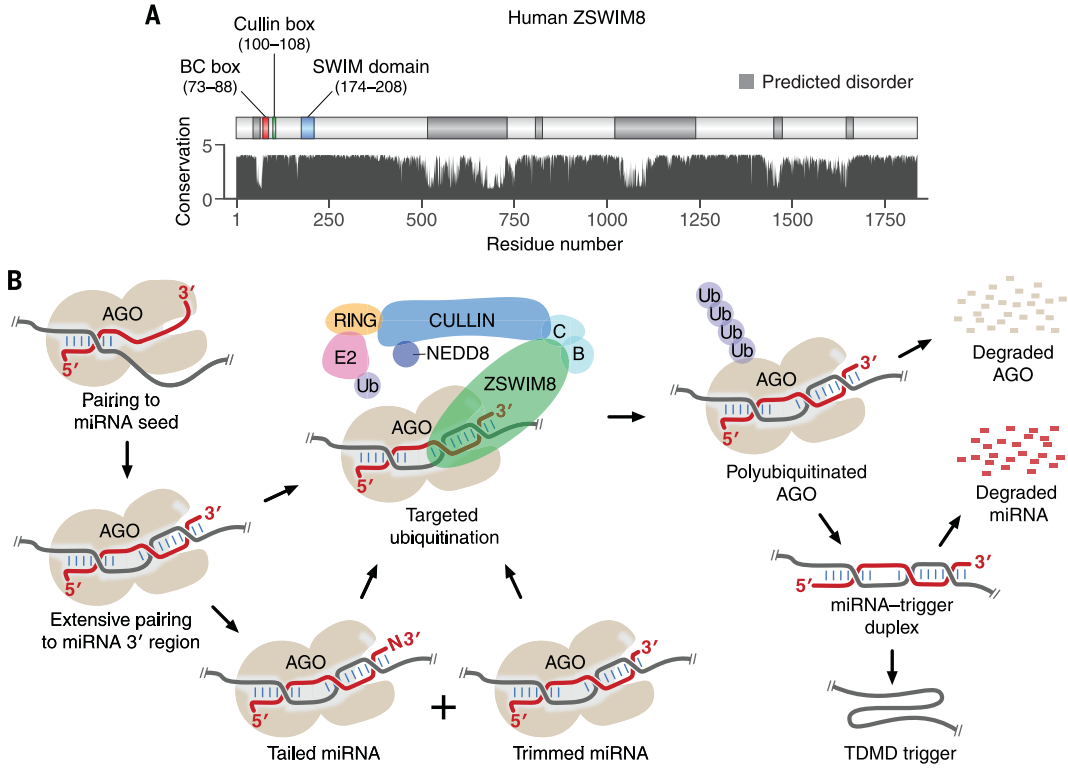

to the miRNA 3′ region, thereby directing the polyubiquitination of AGO, causing it to be degraded by the proteasome. As AGO is proteolyzed, the miRNA is exposed to unknown cellular exonucleases and rapidly degraded, freeing the intact trigger, which resists degradation because it has either a cap and poly(A) tail (e.g., Cyrano) or other stabilizing features (e.g., HSUR1).

Although it differs substantially from the previous model of TDMD, in which tailing marks the miRNA for trimming and ultimately degradation by cellular nucleases without degradation of AGO (*8*, *12*), the E3 model of TDMD is consistent with previous observations concerning both TDMD and TDTT. Like the previous model, the E3 model depends on conformational changes observed upon extensive pairing to the miRNA 3′ region, in which the miRNA 3′ terminus dissociates from its binding pocket in the PAZ domain of AGO and this domain rotates as the channel within the protein widens so that it can accommodate the additional pairing (*8*). However, in the E3 model, the key consequence of these changes is to create a platform for ZSWIM8 association, thereby presenting a degron. Although these changes also expose the miRNA 3′ terminus for TDTT, tailing is not required for degradation in the E3 model, consistent with Cyrano-directed miR-7 degradation in the absence of PAPD4-catalyzed tailing (*21*) (fig. S2D). The E3 model also explains why a specific cellular nuclease required for TDMD has yet to be identified; as AGO is degraded, the exposed miRNA would be the substrate of multiple exonucleases acting redundantly. Finally, release of the intact trigger explains why Cyrano can act with multiple turnover (*21*).

Additional support for the E3 model of TDMD

To investigate a role for other components of the ZSWIM8 CRL in TDMD, we knocked down *ELOB* and *ELOC*. *ELOB* and *ELOC* had respectively scored in the top 0.2% and 12% in our CRISPRi screen (Fig. 1E), but neither was selected as a candidate for secondary screening. Knockdown of each of these adaptor proteins caused miR-7 accumulation to increase, with tailing and trimming resembling that observed after knocking down ZSWIM8 (Fig. 6A and fig. S6A). Likewise, knockdown of the gene encoding Cullin 3 caused increased miR-7 accumulation, which suggested that this protein is also a component of the ZSWIM8 CRL (fig. S6A). As also predicted by the model, general inhibition of ubiquitination activity by TAK-243 (*53*) resulted in the increased accumulation of miR-7 relative to that of a control miRNA (miR-16) (Fig. 6B). Likewise, inhibition of neddylation, which is required for Cullin-mediated ubiquitination, by MLN4924 (*54*) specifically increased miR-7 accumulation, as did inhibition of proteasome-mediated proteolysis by MG-132 (Fig. 6B). Furthermore, the effects of these inhibitors on miR-7 entirely depended on ZSWIM8 function. Thus, ZSWIM8 acts as a component of a CRL to promote TDMD via the ubiquitin-proteasome system.

Another feature of the E3 model is the notion that TDMD does not depend on TDTT. To investigate this idea, we examined the effect of modifying the terminal 2′-OH of miR-7 with a methyl group, which inhibits miRNA tailing and trimming (*12*). Although terminal 2′-O-methylation reduced tailing and trimming of miR-7, it did not reduce the rate of ZSWIM8-dependent miR-7 degradation, which indicated that, as proposed by the model, TDMD does not depend on TDTT (fig. S6B).

To investigate the proposal that the ZSWIM8 CRL polyubiquitinates AGO, we coimmunoprecipitated stabilized polyubiquitinated proteins from both wild-type and *Zswim8*-knockout S2 cells using tagged TUBE (tandem ubiquitin-binding entity) protein (*55*) that we had expressed ectopically in the cells. AGO1 protein (the *Drosophila* AGO ortholog that primarily associates with miRNAs) was not detected by immunoblot analysis of the pull-down samples (fig. S6C); this was attributable, at least in part, to the small fraction of AGO1 loaded with TDMD substrates. Nonetheless, high-throughput sequencing of small RNAs from the polyubiquitinated and input fractions revealed significant enrichment of ZSWIM8-sensitive miRNAs in the polyubiquitinated sample from wild-type cells relative to that from *Zswim8*-knockout cells (Fig. 7A). Moreover, a strong correlation (r^2 = 0.82) was observed between ZSWIM8 sensitivity and differential TUBE enrichment (Fig. 7A). Thus, ZSWIM8 causes preferential association of TDMD substrates with polyubiquitinated proteins (fig. S6D)—a key feature of the E3 model of TDMD.

To test further the idea that these polyubiquitinated proteins were AGO proteins, as would be expected if the ZSWIM8 CRL directly targets AGO proteins during TDMD, we examined the effects of mutating AGO lysines that might serve as sites of ubiquitination. Tagged AGO2 variants possessing lysine-to-arginine substitutions were ectopically expressed in K562i cells, and levels of both miR-7 and a control miRNA (miR-16) that coimmunoprecipitated with each variant were measured. We reasoned that if critical sites of ubiquitination were substituted, then TDMD would be slowed and the relative level of copurifying miR-7 would increase. Of the 53 lysines in human AGO2, 47 were substituted (table S2). The six others, which included three that contact the miRNA 5′ phosphate and three that contact either the miRNA or its target within the seed region (*8*), were not substituted out of concern that they might be required for binding of the miRNA or its targets.

When no lysines were substituted (WT), the ratio of miR-7:miR-16 copurifying from wild-type cells was substantially lower than that observed in *ZSWIM8*-knockout cells (Fig. 7B), as expected from our analyses of cellular miRNA levels (e.g., Fig. 1F). When the 47 lysines were simultaneously substituted (variant R47), the ratio of miR-7:miR-16 copurifying from wild-type cells increased to more closely resemble that observed in *Zswim8*-knockout cells, which indicated that at least one of the 47 substituted lysines was required for efficient degradation of miR-7 (Fig. 7B). The absolute amount of copurifying miRNAs substantially decreased in this highly substituted variant, which was attributed to reduced generic miRNA association rather than reduced production or stability of the protein because this and other lysine-substitution variants each accumulated to a level resembling that of wild-type AGO2 (fig. S7A).

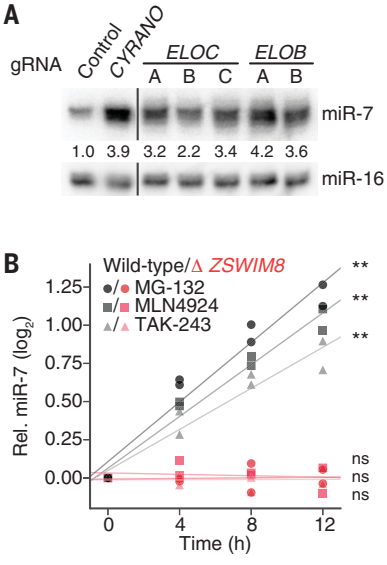

Fig. 6. Additional support for the E3 model of TDMD. (**A**) Influence of *ELOB* and *ELOC* on miR-7 levels in K562i cells. Shown is an RNA blot measuring miR-7 and miR-16 levels in cells expressing either a nontargeting control gRNA or a gRNA targeting either *CYRANO*, *ELOB*, or *ELOC* for CRISPRi-mediated knockdown (fig. S5A). Omitted irrelevant lanes are marked by black lines. Otherwise, as in Fig. 1F. (**B**) Importance of the ubiquitin-proteasome system and the Cullin-RING ligase activity to TDMD. Shown are analyses of RNA blots that measured miR-7 and miR-16 levels after inhibitor treatment of either wild-type (gray) or knockout (Δ*ZSWIM8*, red) clonal K562i lines (table S1A). For each time point of each biological replicate, the signal for miR-7 was normalized to that of miR-16 and then to the miR-7 signal at 0 hours. Lines show the least-squares fit to the results of each treatment. **$p < 0.001$; $n = 2$ biological replicates. MG-132 inhibits the 26*S* proteasome; MLN4924 inhibits Nedd8-activating enzyme (NAE); TAK-243 inhibits ubiquitin-activating enzyme (UAE/E1).

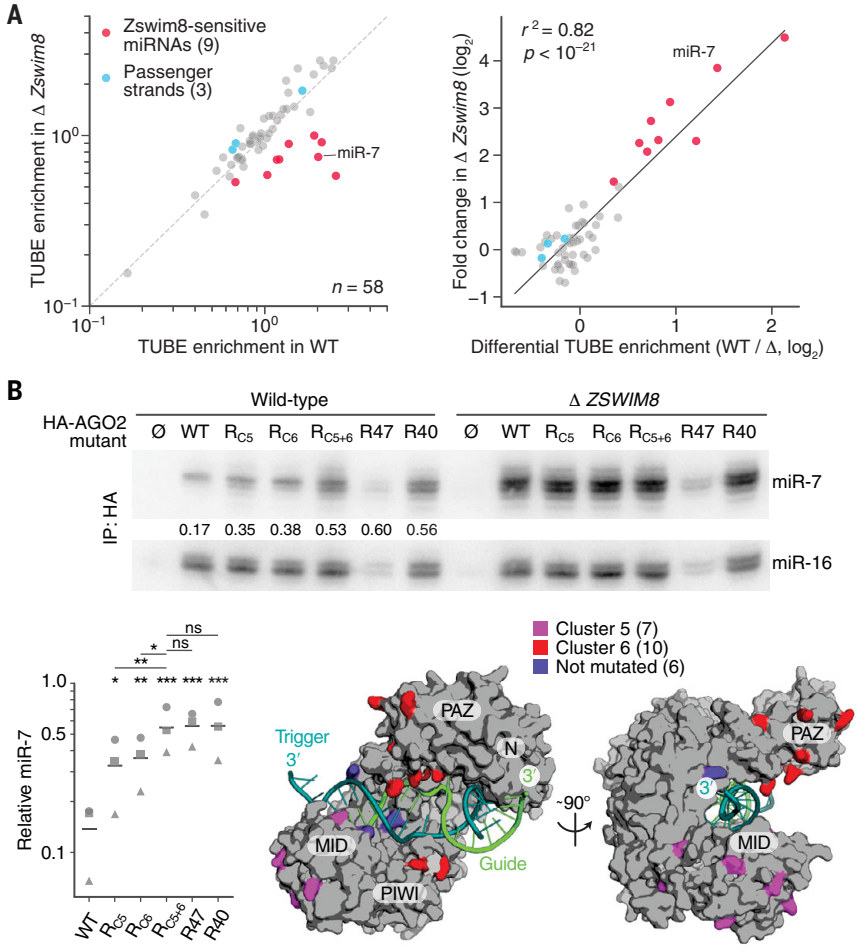

Fig. 7. Evidence for AGO polyubiquitination. (**A**) Physical association between TDMD substrates and polyubiquitinated proteins in S2 cells. Left: Enrichments of miRNAs copurifying with polyubiquitinated proteins, as measured by sRNA-seq of TUBE pull-down and input samples. Results are shown for all miRNAs passing the threshold required for reliable quantification, which included nine ZSWIM8-senstitive miRNAs (red) and three of their passenger strands (blue), plotting mean enrichment in a clonal *CG34401*-knockout S2 line (Δ*Zswim8*) as a function of mean enrichment in an analogously derived clonal wild-type line (WT) (table S1A); $n = 3$ biological replicates. Right: Relationship between ZSWIM8 sensitivity and the mean enrichment observed in TUBE pull-downs from wild-type cells (WT) divided by that observed from Δ*Zswim8* cells (Δ). The line shows the least-squares fit to all data (r^2, coefficient of determination; p value indicated). (**B**) The importance of AGO2 surface lysines for TDMD. Top: RNA blot measuring miR-7 and miR-16 levels in immunoprecipitations from either wild-type or Δ*ZSWIM8* K562i clonal cell lines (table S1A) expressing the indicated 3×HA-tagged protein [Ø, hemagglutinin (HA)–tagged GFP; WT, HA-tagged AGO2; R_X, AGO2 variant with lysine-to-arginine substitutions described in the text]. For each AGO2 variant, the ratio of miR-7:miR-16 observed in a clonal wild-type cell line was normalized to the mean of that observed in three clonal Δ*ZSWIM8* cell lines, and these normalized ratios are shown within each wild-type lane. Lower left: Plot of the same normalized ratios (squares) and results of replicates performed with two other clonal lines (circles and triangles); horizontal lines denote means. *$p < 0.05$, **$p < 0.01$, ***$p < 0.001$ (two-way ANOVA followed by Tukey's multiple-comparisons test). Lower right: Human AGO2 in the TDMD conformation [PDB ID 6MDZ (*8*)], highlighting cluster 5, cluster 6, and unsubstituted lysines. The miRNA (green), TDMD trigger (teal), and AGO domains (N, PAZ, MID, and PIWI) are indicated.

Further analyses examined the effects of substituting clusters of lysines mapping to non-overlapping regions of the protein surface (clusters 1 to 6) (fig. S7B and table S2). These analyses identified a cluster of seven substitutions (cluster 1) in R47 that when reverted to lysines (variant R40) restored miRNA association without restoring miR-7 degradation (Fig. 7B). Furthermore, the lysines required for efficient miR-7 degradation mapped to clusters 5 and 6 (Fig. 7B and fig. S7C, variants R_{C5}, R_{C6}, and R_{C5+6}) yet were not restricted to 10 lysines previously reported to be ubiquitinated (*56*), which had no effect on miR-7 when substituted (fig. S7C, variant R10). Thus, multiple lysines on the AGO2 surface—at least one within cluster 5 and at least one within cluster 6—are important for TDMD. Most important, the ability of these lysine-to-arginine substitutions to phenocopy the *ZSWIM8* knockout with respect to the specific buildup of miR-7, a TDMD substrate, supported our proposal that the ZSWIM8 CRL mediates TDMD through the ubiquitination of AGO. Accordingly, we renamed *CG34401* (the *Drosophila ZSWIM8* ortholog) *Dorado* (*Dora*), after a fish that preys on octopuses from the *Argonauta* genus, following the precedent of the naming of *Iruka* (*Iru*), an E3 ubiquitin ligase that targets empty AGO1 (*57*).

Implications

One of the more surprising features of the E3 mechanism is that it decouples TDMD from TDTT. Despite this decoupling, we anticipate some interplay between TDTT and TDMD. To the extent that these two phenomena act on overlapping substrates, they might compete. Moreover, because slight sequence differences at the miRNA 3′ end can substantially influence the efficiency of TDMD (*8*), some TDTT-mediated 3′-end modifications are expected to either increase or decrease TDMD efficacy.

Our analyses showing that loss of ZSWIM8 caused increased accumulation of 32 miRNAs in MEFs, neurons, or cancer cell lines have substantially expanded the implied scope of endogenous TDMD in mammalian cells, and analogous experiments in *Drosophila* cells and nematodes extended this scope to diverse bilaterian animals. Nonetheless, loss of ZSWIM8 did not influence accumulation of most miRNAs in each of these contexts, which suggests that in most contexts, most miRNAs (which have relatively long half-lives) turn over through another mechanism. Supporting this conclusion, the half-life of AGO2 protein is substantially longer than that of bulk miRNA, implying that for most miRNA-AGO complexes, the miRNA decays first and the protein is recycled (*4*)—a series of events incompatible with that of the E3 TDMD mechanism. Even so, our results indicate that most relatively short-lived miRNAs of each cell type decay through the E3 mechanism.

To the extent that different subsets of miRNAs are short-lived in different cell types, the actual scope of TDMD might be considerably broader than that implied from our study of just a few cell types. In this scenario, different transcripts that trigger TDMD for different miRNAs would be expressed in different cell types, carving away accumulation of specific miRNAs in specific cell types or in response to specific stimuli, thereby creating a more complex and more dynamic landscape of miRNA levels than that which would have been achieved by differential miRNA production alone. Perhaps adding to this complexity are three potential paralogs of ZSWIM8 in mammals (ZSWIM4, ZSWIM5, and ZSWIM6). Although these are more

related to each other than to ZSWIM8 and their expression level appears to be lower than that of ZSWIM8 (median TPM = 4.3, 3.3, 12.9, and 45.2 for *ZSWIM4*, *ZSWIM5*, *ZSWIM6*, and *ZSWIM8*, respectively) (*43*), we are intrigued by the notion that one or more of these potential paralogs might also mediate TDMD, perhaps recognizing unique miRNA-AGO-trigger conformations.

We suspect that each ZSWIM8-sensitive miRNA has at least one target that specifies its degradation. Identifying these TDMD triggers is required for validating the expanded scope of TDMD implied by our results and is critical for exploring the biological roles of the specified degradation. The discovery of ZSWIM8 as an essential mediator of TDMD provides a powerful biochemical and genetic tool for identifying these transcripts that trigger TDMD in different cellular contexts and thereby sculpt miRNA levels throughout the animal.

Methods summary

Gene knockdowns were achieved through CRISPRi. For all knockdown experiments, excluding the CRISPRi screen, stable polyclonal cell lines were generated by transducing K562i cells with a lentivirus that expressed a gRNA and a puromycin-resistance marker under constitutive promoters. Both selection for puromycin resistance and induction of KRAB-dCas9 began 24 hours after transduction and continued for at least 10 days before cells were harvested. Knockdown efficiency was monitored using either RT-qPCR or RNA-seq. Polyclonal knockouts were achieved by transduction with a lentivirus that expressed Cas9, a gRNA, and a puromycin-resistance marker. Selection for puromycin resistance began 24 hours after transduction and continued for at least 10 days before cells were harvested. Polyclonal knockout efficiency was determined by sequencing of a PCR amplicon spanning the targeted region. Clonal knockout cell lines were generated by expression of Cas9 and a gRNA from a transiently transfected (or nucleofected) plasmid, followed by single-cell sorting and then culture and screening of clones.

For RNA-blot analyses, total RNA was resolved on a 15% polyacrylamide denaturing gel, blotted to a membrane, and then chemically cross-linked to the membrane. Membranes were probed with either a ^{32}P-radiolabeled locked nucleic acid corresponding to miR-7 or a ^{32}P-radiolabeled DNA corresponding to another miRNA. The radioactivity was then visualized and quantified using a phosphorimager. For sRNA-seq, sRNAs were gel-purified from each sample and 3′ and 5′ adaptors were sequentially ligated to these sRNAs, which enabled reverse transcription, amplification, and high-throughput sequencing. To reduce biases and enhance reproducibility, the adaptor ligation was performed using an optimized protocol, in which efficiency was monitored using radiolabeled internal standards. The details of each of these methods are described in the supplementary materials.

REFERENCES AND NOTES

1. D. P. Bartel, Metazoan MicroRNAs. *Cell* **173**, 20–51 (2018). doi: 10.1016/j.cell.2018.03.006; pmid: 29570994
2. S. Jonas, E. Izaurralde, Towards a molecular understanding of microRNA-mediated gene silencing. *Nat. Rev. Genet.* **16**, 421–433 (2015). doi: 10.1038/nrg3965; pmid: 26077373
3. R. C. Friedman, K. K.-H. Farh, C. B. Burge, D. P. Bartel, Most mammalian mRNAs are conserved targets of microRNAs. *Genome Res.* **19**, 92–105 (2009). doi: 10.1101/gr.082701.108; pmid: 18955434
4. E. R. Kingston, D. P. Bartel, Global analyses of the dynamics of mammalian microRNA metabolism. *Genome Res.* **29**, 1777–1790 (2019). doi: 10.1101/gr.251421.119; pmid: 31519739
5. B. Reichholf *et al*., Time-Resolved Small RNA Sequencing Unravels the Molecular Principles of MicroRNA Homeostasis. *Mol. Cell* **75**, 756–768.e7 (2019). doi: 10.1016/j.molcel.2019.06.018; pmid: 31350118
6. T. J. Eisen *et al*., The Dynamics of Cytoplasmic mRNA Metabolism. *Mol. Cell* **77**, 786–799.e10 (2020). doi: 10.1016/j.molcel.2019.12.005; pmid: 31902669
7. J. Sheu-Gruttadauria, I. J. MacRae, Structural Foundations of RNA Silencing by Argonaute. *J. Mol. Biol.* **429**, 2619–2639 (2017). doi: 10.1016/j.jmb.2017.07.018; pmid: 28757069
8. J. Sheu-Gruttadauria *et al*., Structural Basis for Target-Directed MicroRNA Degradation. *Mol. Cell* **75**, 1243–1255.e7 (2019). doi: 10.1016/j.molcel.2019.06.019; pmid: 31353209
9. O. S. Rissland, S.-J. Hong, D. P. Bartel, MicroRNA destabilization enables dynamic regulation of the miR-16 family in response to cell-cycle changes. *Mol. Cell* **43**, 993–1004 (2011). doi: 10.1016/j.molcel.2011.08.021; pmid: 21925387
10. J. Krützfeldt *et al*., Specificity, duplex degradation and subcellular localization of antagomirs. *Nucleic Acids Res.* **35**, 2885–2892 (2007). doi: 10.1093/nar/gkm024; pmid: 17439965
11. J. Krützfeldt *et al*., Silencing of microRNAs in vivo with 'antagomirs'. *Nature* **438**, 685–689 (2005). doi: 10.1038/nature04303; pmid: 16258535
12. S. L. Ameres *et al*., Target RNA-directed trimming and tailing of small silencing RNAs. *Science* **328**, 1534–1539 (2010). doi: 10.1126/science.1187058; pmid: 20558712
13. A. Baccarini *et al*., Kinetic analysis reveals the fate of a microRNA following target regulation in mammalian cells. *Curr. Biol.* **21**, 369–376 (2011). doi: 10.1016/j.cub.2011.01.067; pmid: 21353554
14. J. Xie *et al*., Long-term, efficient inhibition of microRNA function in mice using rAAV vectors. *Nat. Methods* **9**, 403–409 (2012). doi: 10.1038/nmeth.1903; pmid: 22388288
15. D. Cazalla, T. Yario, J. A. Steitz, Down-regulation of a host microRNA by a Herpesvirus saimiri noncoding RNA. *Science* **328**, 1563–1566 (2010). doi: 10.1126/science.1187197pmid: 20558719
16. V. Libri *et al*., Murine cytomegalovirus encodes a miR-27 inhibitor disguised as a target. *Proc. Natl. Acad. Sci. U.S.A.* **109**, 279–284 (2012). doi: 10.1073/pnas.1114204109; pmid: 22184245
17. L. Marcinowski *et al*., Degradation of cellular mir-27 by a novel, highly abundant viral transcript is important for efficient virus replication in vivo. *PLOS Pathog.* **8**, e1002510 (2012). doi: 10.1371/journal.ppat.1002510; pmid: 22346748
18. S. Lee *et al*., Selective degradation of host MicroRNAs by an intergenic HCMV noncoding RNA accelerates virus production. *Cell Host Microbe* **13**, 678–690 (2013). doi: 10.1016/j.chom.2013.05.007; pmid: 23768492
19. A. Bitetti *et al*., MicroRNA degradation by a conserved target RNA regulates animal behavior. *Nat. Struct. Mol. Biol.* **25**, 244–251 (2018). doi: 10.1038/s41594-018-0032-x; pmid: 29483647
20. F. Ghini *et al*., Endogenous transcripts control miRNA levels and activity in mammalian cells by target-directed miRNA degradation. *Nat. Commun.* **9**, 3119 (2018). doi: 10.1038/s41467-018-05182-9; pmid: 30087332
21. B. Kleaveland, C. Y. Shi, J. Stefano, D. P. Bartel, A Network of Noncoding Regulatory RNAs Acts in the Mammalian Brain. *Cell* **174**, 350–362.e17 (2018). doi: 10.1016/j.cell.2018.05.022; pmid: 29887379
22. D. P. Bartel, MicroRNAs: Target recognition and regulatory functions. *Cell* **136**, 215–233 (2009). doi: 10.1016/j.cell.2009.01.002; pmid: 19167326
23. M. de la Mata *et al*., Potent degradation of neuronal miRNAs induced by highly complementary targets. *EMBO Rep.* **16**, 500–511 (2015). doi: 10.15252/embr.201540078; pmid: 25724380
24. R. Denzler *et al*., Impact of MicroRNA Levels, Target-Site Complementarity, and Cooperativity on Competing Endogenous RNA-Regulated Gene Expression. *Mol. Cell* **64**, 565–579 (2016). doi: 10.1016/j.molcel.2016.09.027; pmid: 27871486
25. G. Haas *et al*., Identification of factors involved in target RNA-directed microRNA degradation. *Nucleic Acids Res.* **44**, 2873–2887 (2016). doi: 10.1093/nar/gkw040; pmid: 26809675
26. P. Pawlica, J. Sheu-Gruttadauria, I. J. MacRae, J. A. Steitz, How Complementary Targets Expose the microRNA 3′ End for Tailing and Trimming during Target-Directed microRNA Degradation. *Cold Spring Harb. Symp. Quant. Biol.* **84**, 179–183 (2019). pmid: 32019864
27. I. Heo *et al*., Lin28 mediates the terminal uridylation of let-7 precursor MicroRNA. *Mol. Cell* **32**, 276–284 (2008). doi: 10.1016/j.molcel.2008.09.014; pmid: 18951094
28. S. Vaňáčová, *et al*., A new yeast poly(A) polymerase complex involved in RNA quality control. *PLOS Biol.* **3**, e189 (2005). doi: 10.1371/journal.pbio.0030189; pmid: 15828860
29. J. LaCava *et al*., RNA degradation by the exosome is promoted by a nuclear polyadenylation complex. *Cell* **121**, 713–724 (2005). doi: 10.1016/j.cell.2005.04.029; pmid: 15935758
30. F. Wyers *et al*., Cryptic pol II transcripts are degraded by a nuclear quality control pathway involving a new poly(A) polymerase. *Cell* **121**, 725–737 (2005). doi: 10.1016/j.cell.2005.04.030; pmid: 15935759
31. O. S. Rissland, C. J. Norbury, Decapping is preceded by 3′ uridylation in a novel pathway of bulk mRNA turnover. *Nat. Struct. Mol. Biol.* **16**, 616–623 (2009). doi: 10.1038/nsmb.1601; pmid: 19430462
32. J. Lim *et al*., Uridylation by TUT4 and TUT7 marks mRNA for degradation. *Cell* **159**, 1365–1376 (2014). doi: 10.1016/j.cell.2014.10.055; pmid: 25480299
33. T. E. Mullen, W. F. Marzluff, Degradation of histone mRNA requires oligouridylation followed by decapping and simultaneous degradation of the mRNA both 5′ to 3′ and 3′ to 5′. *Genes Dev.* **22**, 50–65 (2008). doi: 10.1101/gad.1622708; pmid: 18172165
34. M.-G. Song, M. Kiledjian, 3′ Terminal oligo U-tract-mediated stimulation of decapping. *RNA* **13**, 2356–2365 (2007). doi: 10.1261/rna.765807; pmid: 17942740
35. J. Li, Z. Yang, B. Yu, J. Liu, X. Chen, Methylation protects miRNAs and siRNAs from a 3′-end uridylation activity in Arabidopsis. *Curr. Biol.* **15**, 1501–1507 (2005). doi: 10.1016/j.cub.2005.07.029; pmid: 16111943
36. A. M. Burroughs *et al*., A comprehensive survey of 3′ animal miRNA modification events and a possible role for 3′ adenylation in modulating miRNA targeting effectiveness. *Genome Res.* **20**, 1398–1410 (2010). doi: 10.1101/gr.106054.110; pmid: 20719920
37. F. Mansur *et al*., Gld2-catalyzed 3′ monoadenylation of miRNAs in the hippocampus has no detectable effect on their stability or on animal behavior. *RNA* **22**, 1492–1499 (2016). doi: 10.1261/rna.056937.116; pmid: 27495319
38. S. Shukla, G. A. Bjerke, D. Muhlrad, R. Yi, R. Parker, The RNase PARN Controls the Levels of Specific miRNAs that Contribute to p53 Regulation. *Mol. Cell* **73**, 1204–1216.e4 (2019). doi: 10.1016/j.molcel.2019.01.010; pmid: 30770239
39. L. A. Gilbert *et al*., CRISPR-mediated modular RNA-guided regulation of transcription in eukaryotes. *Cell* **154**, 442–451 (2013). doi: 10.1016/j.cell.2013.06.044; pmid: 23849981
40. M. A. Horlbeck *et al*., Compact and highly active next-generation libraries for CRISPR-mediated gene repression and activation. *eLife* **5**, e19760 (2016). doi: 10.7554/eLife.19760; pmid: 27661255
41. W. Li *et al*., MAGeCK enables robust identification of essential genes from genome-scale CRISPR/Cas9 knockout screens. *Genome Biol.* **15**, 554 (2014). doi: 10.1186/s13059-014-0554-4; pmid: 25476604
42. L. A. Gilbert *et al*., Genome-Scale CRISPR-Mediated Control of Gene Repression and Activation. *Cell* **159**, 647–661 (2014). doi: 10.1016/j.cell.2014.09.029; pmid: 25307932
43. J. Lonsdale *et al*., The Genotype-Tissue Expression (GTEx) project. *Nat. Genet.* **45**, 580–585 (2013). doi: 10.1038/ng.2653; pmid: 23715323
44. Z. Wang *et al*., The EBAX-type Cullin-RING E3 ligase and Hsp90 guard the protein quality of the SAX-3/Robo receptor in developing neurons. *Neuron* **79**, 903–916 (2013). doi: 10.1016/j.neuron.2013.06.035; pmid: 24012004

45. M. Stoeckius *et al*., Large-scale sorting of C. elegans embryos reveals the dynamics of small RNA expression. *Nat. Methods* **6**, 745–751 (2009). doi: 10.1038/nmeth.1370; pmid: 19734907
46. W. P. Schreiner *et al*., Remodeling of the Caenorhabditis elegans non-coding RNA transcriptome by heat shock. *Nucleic Acids Res.* **47**, 9829–9841 (2019). doi: 10.1093/nar/gkz693; pmid: 31396626
47. R. I. Enchev, B. A. Schulman, M. Peter, Protein neddylation: Beyond cullin-RING ligases. *Nat. Rev. Mol. Cell Biol.* **16**, 30–44 (2015). doi: 10.1038/nrm3919; pmid: 25531226
48. Z. Hua, R. D. Vierstra, The cullin-RING ubiquitin-protein ligases. *Annu. Rev. Plant Biol.* **62**, 299–334 (2011). doi: 10.1146/annurev-arplant-042809-112256; pmid: 21370976
49. N. Mahrour *et al*., Characterization of Cullin-box sequences that direct recruitment of Cul2-Rbx1 and Cul5-Rbx2 modules to Elongin BC-based ubiquitin ligases. *J. Biol. Chem.* **283**, 8005–8013 (2008). doi: 10.1074/jbc.M706987200; pmid: 18187417
50. K. S. Makarova, L. Aravind, E. V. Koonin, SWIM, a novel Zn-chelating domain present in bacteria, archaea and eukaryotes. *Trends Biochem. Sci.* **27**, 384–386 (2002). doi: 10.1016/S0968-0004(02)02140-0; pmid: 12151216
51. S. Yamamoto *et al*., A Drosophila genetic resource of mutants to study mechanisms underlying human genetic diseases. *Cell* **159**, 200–214 (2014). doi: 10.1016/j.cell.2014.09.002; pmid: 25259927
52. DepMap 20Q2 Public (2020); doi:10.6084/m9.figshare.12280541.v3.
53. M. L. Hyer *et al*., A small-molecule inhibitor of the ubiquitin activating enzyme for cancer treatment. *Nat. Med.* **24**, 186–193 (2018). doi: 10.1038/nm.4474; pmid: 29334375
54. T. A. Soucy *et al*., An inhibitor of NEDD8-activating enzyme as a new approach to treat cancer. *Nature* **458**, 732–736 (2009). doi: 10.1038/nature07884; pmid: 19360080
55. Y. Yoshida *et al*., A comprehensive method for detecting ubiquitinated substrates using TR-TUBE. *Proc. Natl. Acad. Sci. U.S.A.* **112**, 4630–4635 (2015). doi: 10.1073/pnas.1422313112; pmid: 25827227
56. P. V. Hornbeck *et al*., PhosphoSitePlus: A comprehensive resource for investigating the structure and function of experimentally determined post-translational modifications in man and mouse. *Nucleic Acids Res.* **40**, D261–D270 (2012). doi: 10.1093/nar/gkr1122; pmid: 22135298
57. H. Kobayashi, K. Shoji, K. Kiyokawa, L. Negishi, Y. Tomari, Iruka Eliminates Dysfunctional Argonaute by Selective Ubiquitination of Its Empty State. *Mol. Cell* **73**, 119–129.e5 (2019). doi: 10.1016/j.molcel.2018.10.033; pmid: 30503771
58. D. Piovesan *et al*., MobiDB 3.0: More annotations for intrinsic disorder, conformational diversity and interactions in proteins. *Nucleic Acids Res.* **46**, D471–D476 (2018). doi: 10.1093/nar/gkx1071; pmid: 29136219
59. C. Berezin *et al*., ConSeq: The identification of functionally and structurally important residues in protein sequences. *Bioinformatics* **20**, 1322–1324 (2004). doi: 10.1093/bioinformatics/bth070; pmid: 14871869

ACKNOWLEDGMENTS

We thank S. McGeary and X. Wu for helpful discussions; A. Liu, A. Whipple, J. Steitz, T. Pham, J. Weissman, P. Sharp, D. Trono, D. Sabatini, S. Lindquist, M. Taipale, Y. Doyon, and Y. Saeki for cell lines and plasmids; Y. Jin and S. Mitani for *C. elegans* strains; the Whitehead Functional Genomics Core for support with the CRISPRi screen; and the Whitehead Genome Technology Core for sequencing. **Funding:** Supported by NIH grant GM118135 (D.P.B.) and a NSF predoctoral GRFP fellowship (E.R.K.). D.H.L. is an HHMI fellow of the Damon Runyon Cancer Research Foundation (DRG-2345-18). D.P.B. is an investigator of the Howard Hughes Medical Institute. **Author contributions:** C.Y.S. performed experiments using K562, BJAB, and mouse cells; E.R.K., B.K., and M.W.S. performed experiments using *Drosophila* cells, other human cancer lines, and nematodes, respectively; C.Y.S., E.R.K., B.K., D.H.L., and D.P.B. designed the study; and C.Y.S. and D.P.B. wrote the manuscript with input from the other authors. **Competing interests:** D.P.B. has equity in Alnylam Pharmaceuticals, where he is a co-founder and advisor. The other authors declare no competing interests. **Data and materials availability:** Sequencing data and associated analyses were deposited in Gene Expression Omnibus (accession number GSE160304), and all plasmids generated in this study were submitted to Addgene.

SUPPLEMENTARY MATERIALS

21 May 2020; resubmitted 7 September 2020
Accepted 29 October 2020
Published online 12 November 2020
10.1126/science.abc9359

The ZSWIM8 ubiquitin ligase mediates target-directed microRNA degradation

Charlie Y. Shi, Elena R. Kingston, Benjamin Kleaveland, Daniel H. Lin, Michael W. Stubna, and David P. Bartel

Science, **370** (6523), eabc9359.
DOI: 10.1126/science.abc9359

Turning the tables on microRNA decay

MicroRNAs help to regulate many genes in animal cells. Each microRNA associates with an Argonaute (AGO) protein, forming a complex in which the microRNA pairs with a messenger RNA (mRNA) target and AGO recruits factors that accelerate mRNA decay. However, for some unusual targets, the reverse occurs: Pairing to the target recruits factors that accelerate microRNA decay rather than degradation of the mRNA. Working independently, Shi *et al.* and Han *et al.* elucidate the mechanism of this phenomenon. They found that pairing to the unusual targets recruits a ubiquitin ligase that causes degradation of AGO, thereby exposing the microRNA to cellular nucleases. Mutating the ubiquitin ligase in diverse animals and cell types deregulates numerous microRNAs, implying that this phenomenon is widely deployed to sculpt microRNA levels.

Science, this issue p. eabc9359, p. eabc9546